Available online at www.sciencedirect.com
SCIENCE DIRECT®
Journal of Luminescence 107 (2004) 314–331
JOURNAL OF LUMINESCENCE
www.elsevier.com/locate/jlumin

# Incorporating excitation-induced dephasing into the Maxwell–Bloch numerical modeling of photon echoes

Geoffrey W. Burr[a,*], Todd L. Harris[b], Wm. Randall Babbitt[b], C. Michael Jefferson[a]

[a] IBM Almaden Research Center, 650 Harry Road, San Jose, CA 95120, USA
[b] The Spectrum Lab, Montana State University, P.O. Box 173510 Bozeman, MT 59717, USA

**Abstract**

We describe the incorporation of excitation-induced dephasing (EID) into the Maxwell–Bloch numerical simulation of photon echoes. At each time step of the usual numerical integration, stochastic frequency jumps of ions—caused by excitation of neighboring ions—is modeled by convolving each Bloch vector with the Bloch vectors of nearby frequency detunings. The width of this convolution kernel follows the instantaneous change in overall population, integrated over the simulated bandwidth. This approach is validated by extensive comparison against published and original experimental results. The enhanced numerical model is then used to investigate the accuracy of experiments designed to extrapolate to the intrinsic dephasing time $T_2$ from data taken in the presence of EID. Such a modeling capability offers improved understanding of experimental results, and should allow quantitative analysis of engineering tradeoffs in realistic optical coherent transient applications.


*PACS:* 42.50.Md; 02.60.Cb

*Keywords:* Optical transient phenomena; Quantum beats; Photon echo; Free-induction decay; De-phasings and revivals; Optical nutation; Self-induced transparency; Numerical simulation; Solution of equations

## 1. Introduction

In an inhomogeneously broadened material, such as those used for spectral-hole burning or coherent transients, each dopant ion has a narrow resonance frequency (or *homogeneous* linewidth) dictated by its local neighborhood. The unique properties of these materials for storage and data processing applications [1–4] arise from the combination of this narrow homogeneous line width, a broad distribution of such resonances (the *inhomogeneous* line width), and long coherence times (the time during which the ions that share a resonance frequency respond collectively).

However, optical excitation of other ions within an ion's local neighborhood can shift its resonance frequency [5–10] due to changes in static electric–dipole moment [7], magnetic dipole–dipole interaction [9], or even lattice vibration [11,12]. These effects are often viewed as being the optical analog to the instantaneous diffusion seen in nuclear magnetic resonance [13,14]. During a photon echo,

*Corresponding author. Tel.: +1-408-927-1512; fax: +1-408-927-2100.
*E-mail address:* burr@almaden.ibm.com (G.W. Burr).

0022-2313/$ - see front matter © 2003 Elsevier B.V. All rights reserved.
doi:10.1016/j.jlumin.2003.12.034

such frequency shifts lead to an additional loss of coherence known as excitation-induced dephasing (EID) or instantaneous spectral diffusion. As a result, the measured photon echo decay rate depends on the excitation intensity, in contrast to the predictions of the standard optical Bloch equations [15,16]. (Similar intensity-dependent decays can also occur during free-induction decay [17,18].) A summary of EID observations in photon echoes (as of 1996) can be found in Ref. [19].

In an engineering sense, the presence of a dephasing time $T_2$ already limits the maximum time delay between two pulses that can be stored or processed with a coherent transient system. Given that the maximum bandwidth is determined by—absent other limiting effects—the inhomogeneous line width, the effect of $T_2$ is to set the maximum time–bandwidth product and thus the number of data bits that can be stored or processed. The additional presence of EID introduces a set of complex and undesired tradeoffs in such systems: increasing either the signal-strength (by increasing the excitation per bandwidth) or the bandwidth itself leads to a decrease in the effective dephasing time. Thus trying for more signal or more bandwidth can lead to less data stored (or processed) overall. As a result, EID can severely impact the use of such spectrally sensitive materials in coherent transient storage and signal processing applications.

Conversely, such strong ion–ion coupling might be useful for communicating quantum state information between optically accessible ions for solid-state quantum computation [20,21]. In these proposed schemes, it is the same dipole–dipole coupling between ions that causes EID which is called upon to enable the communication between qubits. By putting the "control" ion into its upper state, the resonance frequency of the nearby "data" ion shifts slightly. Thus one of the important requirements of quantum computation—a basic 2-qubit gate such as the 'controlled-NOT' [22]—could potentially be implemented.

As a result, a better understanding of EID would facilitate engineering tradeoff analysis and optimization not only for applications where EID limits system performance, but also for those where EID enables novel functionality. Here we describe the incorporation of EID directly into the numerical integration of the Maxwell–Bloch equations. This allows modeling of arbitrary pulse inputs (including chirps) in media that can be also optically thick, and should make it possible to identify more of the underlying physics from experimental results than has previously been possible. In addition, such a modeling capability could make it possible to quantitatively evaluate engineering tradeoffs between time, bandwidth, and signal strength that were previously inaccessible, within the time–bandwidth limitations of these simulations.

## 2. Excitation-induced dephasing

A vivid example of such tradeoffs between time, bandwidth, and signal strength is shown in Fig. 1, where experimental photon echo measurements are compared with the predictions of conventional Maxwell–Bloch modeling.

Fig. 1(a) shows the measured photon echo intensity due to a linear frequency chirp followed by a transform-limited *cw* $\pi$ pulse, as a function of the chirp intensity. The chirp intensity shown on the horizontal axis has been normalized by the intensity at which the envelope of the transmitted probe pulse remains flat, as described in Ref. [23]. This condition is met when absorption and stimulated emission are balanced (as averaged through the depth of the media), and indicates that an equal mixture of ground and excited states have been excited (e.g., the $r_3$ component of the Bloch vector, averaged over depth, is zero). Since this condition is identical to the on-resonant behavior after a *cw* $\pi/2$ pulse, it might be expected that this level of chirped excitation should lead to a maximal photon echo signal (assuming low optical density and non-interacting ions). And at low chirp bandwidth (top curve of Fig. 1), this expectation holds true. But as the chirp bandwidth increases, the photon echo signal decreases with chirp intensity as well as with chirp bandwidth.

We attribute this intensity- and bandwidth-dependent photon echo signal to EID [6–10]. In

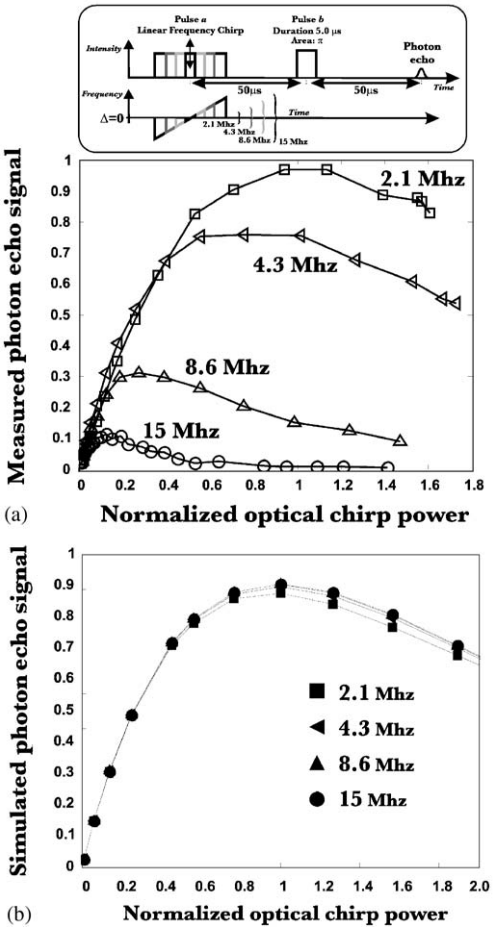


Fig. 1. (a) Measured two-pulse photon echo intensity for a linear frequency chirp followed by a *cw* probe at the chirp center, plotted as a function of the normalized chirp power for various chirp bandwidths. Data taken using a frequency- and amplitude-stabilized dye laser at 579.879 nm in a $Eu^{3+}$: $Y_2SiO_5$ crystal of optical density $\alpha L = 1.2$ [23]. The linear chirp is of constant chirp rate (15 MHz/70 μs), so lower bandwidth means shorter chirp duration; the 5.0 μs probe pulse is always a $\pi$ pulse, centered 50 μs after the center of the chirp. (b) Simulated two-pulse photon echo for the same experiment, using a conventional Maxwell–Bloch numerical model (same as in Ref. [23], with $T_1 = 2$ ms, $T_2 = 500$ μs, intensity $\alpha = 4.6$ cm$^{-1}$, and thickness = 0.26 cm). In both parts, lines are present only to guide the eye.

a simplistic description of a two-pulse photon echo (Fig. 2(a)) operating on an inhomogeneously broadened distribution of absorbers (Fig. 2(b)), the time-evolution of the phase of the atomic coherences can be pictured as a series of straight

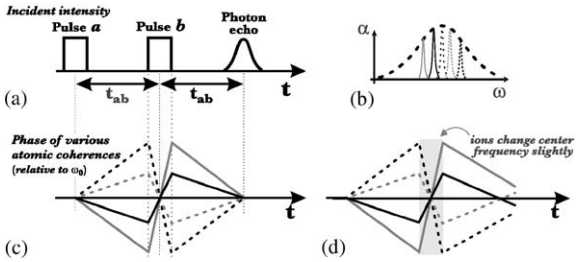


Fig. 2. Given a two-pulse photon echo (a) operating on an inhomogeneously broadened distribution of absorbers (b), the time-evolution of the phase of the participating atomic coherences (c) can be pictured as a series of straight lines. After the application of a second pulse and the rephasing of the coherences, a photon echo will be produced. In the presence of EID, however, the second pulse perturbs the resonance frequencies (d), leading to imperfect rephasing and a weaker photon echo.

lines (Fig. 2(c)). Since each ion resonates at a slightly different frequency, its overall phase pulls steadily away from the baseline phase of the central excitation frequency. A second pulse, of area $\pi$, can flip the phase of the ions so that their subsequent progression brings them all back into phase, at which point the resulting macroscopic polarization can lead to emission of a photon echo. In the presence of EID (Fig. 2(d)), the excitation caused by the second pulse (or in the case of the experiment shown in Fig. 1(a), by the latter half of the linear frequency chirp) can cause small jumps in the resonance frequencies for some of the (physically neighboring) ions participating in the photon echo. Thus the phase that was wound up at one rate is unwound at another, leading to imperfect rephasing and a weaker photon echo. Intuitively, the point at which such frequency jumps will have the strongest effect is during the second pulse, since then the accumulated phase error at the photon echo is maximized.

Unfortunately, this graphical approach to describing EID is limited, since it would be difficult to extend it beyond pulses that are short compared to the delays between pulses, or to include off-resonant or other bandwidth effects, or to model chirps, or to include propagation effects. However, there is a model which does include all these effects: numerical integration of the Maxwell–Bloch equations [16,24–27]. But this basic

modeling tool—used to simulate many coherent transient devices in optically thick media [24–27]—does not include the effects of EID. This is vividly demonstrated in Fig. 1(b), where the predictions of a conventional Maxwell–Bloch simulator are shown for the same four experiments as Fig. 1(a). Since the model incorporates only a constant dephasing time $T_2$, none of the excitation-dependent effects that dominate this particular experiment are represented.

The purpose of this paper is to remedy this situation: to incorporate EID into the Maxwell–Bloch modeling of photon echoes. In Section 3, we describe the conventional Maxwell–Bloch numerical model, and discuss a few relevant issues that have not been addressed before in the literature. In Section 4, our method for incorporating EID is described, followed in Section 5 by a description of a typical photon echo simulation. Section 6 is dedicated to verifying the EID model by comparison against photon echo decay experiments, both from the literature as well as from our own experiments (Fig. 1). In Section 7, we use the numerical model to investigate the accuracy of experiments that are designed to extrapolate to the intrinsic value of $T_2$ despite the unavoidable presence of EID. Section 8 is a discussion of experimental situations that are not (yet) handled correctly by the EID/Maxwell–Bloch model as it currently stands, and finally, Section 9 concludes the paper with a discussion of possible avenues for future work.

## 3. The "conventional" Maxwell–Bloch model

The simulations described here model the interaction of an optically thick inhomogeneously broadened ensemble of two-level atomic systems with a plane wave near-monochromatic optical input. Our implementation follows an approach that has been used by several researchers to model the response of such media to both single-frequency and chirped pulses [24–27]. In particular, this conventional model is identical to the one used in Ref. [23]. Extensions of this Maxwell–Bloch model to beams with Gaussian spatial profiles, and to multiple beams of different angle of incidence have recently been demonstrated [28,29].

To begin, the localized quantum state of each individual two-level system with unique resonance frequency $\omega$ is described by its density matrix $\rho$. The time evolution of the density matrix given a Hamiltonian $H$ is derived from Schrödinger's equation as

$$\frac{\partial \rho}{\partial t} = \frac{i}{\hbar}[\rho, H], \tag{1}$$

where $\hbar$ is Planck's constant divided by $2\pi$ and the brackets here represent a commutator. In turn, by using a frame of reference rotating at a nearby frequency $\omega_0$, the density matrix can be reduced to three components forming a virtual "Bloch vector" that describes the state of the two-level system:

$$\begin{aligned} r_1 &= 2\ \mathrm{Re}\{\rho_{12}\}, \\ r_2 &= 2\,\mathrm{Im}\{\rho_{12}\}, \\ r_3 &= 1 - 2\rho_{11}. \end{aligned} \tag{2}$$

Here, $r_3$ represents the occupancy of the ground and excited states ($-1$ when fully in the ground state, $+1$ in the excited state), and $r_1$ and $r_2$ represent the coherent oscillation between these states. If the aggregate oscillation of all two-level systems of various $\omega$ are in phase, then the resulting macroscopic polarization $P(z,t)$ can serve as the driving term in the wave equation

$$\nabla^2 E(z,t) - \frac{n^2}{c^2}\frac{\partial^2}{\partial t^2} E(z,t) = \mu_0 \frac{\partial^2}{\partial t^2} P(z,t), \tag{3}$$

providing the "Maxwell" portion of the simulation. Here, $n$ is the index of refraction, $c$ the speed of light, and $\mu_0$ the permittivity of free space. The incident electromagnetic field is assumed to be a nearly monochromatic plane wave propagating along $z$ with an envelope that varies slowly in both space and time,

$$\begin{aligned} E(z,t) = \frac{\hbar}{\mu_{12}}[&\Omega_r(z,t)\cos(\omega_0 t - kz) \\ &- \Omega_i(z,t)\sin(\omega_0 t - kz)], \end{aligned} \tag{4}$$

where $\mu_{12}$ is the transition dipole moment of the two-level system, $k$ is the wavevector, and $\Omega_{r,i}$ are Rabi frequencies in units of $[\mathrm{s}^{-1}]$. These latter terms can be considered as a

"material-reduced" incident electrical field, or as the "Rabi frequency of the pulse" [23]. This concept is useful in dealing with off-resonant interactions with *cw* pulses and complicated modulations such as chirps [23].

The combination of Eqs. (1)–(4) lead to the following five coupled Maxwell–Bloch equations (see Refs. [26,27] for details of the derivation):

$$\frac{\partial r_1(z,t',\Delta)}{\partial t'} = \Delta r_2(z,t',\Delta) - \Omega_i(z,t')r_3(z,t',\Delta) - \frac{r_1(z,t',\Delta)}{T_2},$$

$$\frac{\partial r_2(z,t',\Delta)}{\partial t'} = -\Delta r_1(z,t',\Delta) + \Omega_r(z,t')r_3(z,t',\Delta) - \frac{r_2(z,t',\Delta)}{T_2},$$

$$\frac{\partial r_3(z,t',\Delta)}{\partial t'} = -\Omega_r(z,t')r_2(z,t',\Delta) + \Omega_i(z,t')r_1(z,t',\Delta) - \frac{1+r_3(z,t',\Delta)}{T_1}, \quad (5)$$

$$\frac{\partial \Omega_r(z,t')}{\partial z} = \frac{\alpha}{4\pi}\int_{-\infty}^{\infty} r_2(z,t',\Delta)g(\Delta)\,\mathrm{d}\Delta,$$

$$\frac{\partial \Omega_i(z,t')}{\partial z} = -\frac{\alpha}{4\pi}\int_{-\infty}^{\infty} r_1(z,t',\Delta)g(\Delta)\,\mathrm{d}\Delta. \quad (6)$$

Here $\Delta = \omega - \omega_0$ is the detuning from the frequency of the rotating frame, $T_1$ and $T_2$ are the excited-state lifetime and dephasing time, respectively, and $g(\Delta)$ describes the relative line shape of the (intensity) absorption coefficient $\alpha$ in the local vicinity of $\omega_0$. To avoid having both space and time derivatives of $\Omega_{r,i}$, we have converted from the original time $t$ to a travelling frame $t' = t - (n/c)z$, such that an optical pulse starting at $t = z = 0$ reaches each $z$ slice at time $t' = 0$ [24]. Note that by having pulled out the material parameter $\mu_{12}$ in Eq. (4), the material-dependent parameters in Eqs. (5) and (6) are simply $T_1$, $T_2$, $\alpha$, and $g(\Delta)$.

The final terms on each line of Eq. (5) induce an exponential decay back to the steady-state condition of $r_1 = r_2 = 0, r_3 = -1$. The elegance of describing excitation in terms of Rabi frequencies is revealed by the Bloch vector response at $\Delta = 0$ to a constant input of $\Omega_r$: ignoring the impact of $T_1$ and $T_2$, the coupling between $r_2$ and $r_3$ causes the latter (which again describes the degree to which the two-level system is in the ground or excited states) to simply oscillate as $-\cos(\Omega_r t')$. This also explains the origin of the term "pulse area" to describe the quantity $\int \Omega_r\,\mathrm{d}t$.

Numerical solution of Eqs. (5) and (6) is simplified by assuming causality and the absence of back-reflection. Thus $t'$ and $z$ can simply be incremented in two nested loops, with the innermost loop evaluating Eq. (5) at each $\Delta$, followed by evaluation of Eq. (6) to compute the media's effect on the field for the next deeper $z$.

Readers wishing to duplicate this implementation can use the C++ code in the Appendix of Ref. [26] as a starting point with the following minor modifications:

(1) The addition of $\Omega_i$ terms as shown above to allow the input of chirped input pulses, written as

$$E \sim \cos\left((\omega_0+\omega_1)t + \frac{A}{2}t^2\right) = \cos\left(\omega_1 t + \frac{A}{2}t^2\right)\cos(\omega_0 t) - \sin\left(\omega_1 t + \frac{A}{2}t^2\right)\sin(\omega_0 t), \quad (7)$$

so that the instantaneous frequency at time $t$ is $\omega_1 + At$ (primes dropped for readability).

(2) The re-ordering of the two outer loops with the $z$ loop outermost. This change allows $\Omega_{r,i}$ and $r_{1,2,3}$ to be stored as simple vectors (of $t'$ and $\Delta$ respectively) rather than as arrays (varying along $z$ as well). The resulting savings in computer memory permit much larger simulations to be run, limited only by execution time.

(3) For numerical stability in the integration, two copies of $r_{1,2,3}$ are kept and updated in leapfrog manner [26]. But it is important that the copy that is integrated in Eq. (6) to compute the macroscopic polarization corresponds to the current time-slot (rather than the next time-slot), lest the media contribution to the electric field be applied out-of-phase. With chirped input pulses, this can lead to the simulation

producing un-physical increases in transmitted field as $t'$ and $z$ progress.

The final issue in the numerical simulation is the choice of range and sampling along the three variables of interest: $z$, $t'$, and $\Delta$. The time and space extent of the simulation, $L$ and $t_{\text{final}}$ respectively, are determined by the crystal thickness and pulse sequence to be simulated. The frequency extent of the simulation ($\Delta_{\max}$) is chosen so that the contribution of $r_{1,2}$ to the integrals in Eq. (6) from the maximum detunings is negligible. The sampling along $z$ is typically selected to keep the step in $\alpha z$ to $<0.05$, which has been previously found to be sufficient to keep simulation results independent of the exact sampling [30].

In contrast, however, the required sampling in frequency and time can be specified much more precisely. For instance, the required sampling along frequency must be sufficient to resolve the frequency grating formed by pulses at $t = 0$ and $t = 0.5t_{\text{final}}$, in order to correctly replay the photon echo expected near $t = t_{\text{final}}$. (As $t_{\text{final}}$ grows much larger than $T_2$, this constraint can be relaxed, since any such high-frequency grating would be suppressed by loss of coherence.) Thus, the frequency range must be divided into at least $2t_{\text{final}}\Delta_{\max}$ slots (essentially the time–bandwidth product of the simulation). In turn, the time resolution must be sufficient to follow the fastest Bloch vector rotation, given the combined effects of $\Delta$ and time-varying $\Omega_{r,i}$ in Eq. (5). This requires that the

$$\#\ \text{of timeslots} = 2\pi t_{\text{final}}(\Delta_{\max} + \omega_1), \tag{8}$$

where $\omega_1$ represents the maximum frequency excursion of any chirped excitation from the center frequency $\Delta = 0$. These guidelines can easily be extended to the case where the simulated frequency bandwidth is not centered on $\Delta = 0$.

In the case of strong excitation, the magnitude of $\Omega_{r,i}$ in Eq. (5) may be large enough that this minimum time step may need to be further reduced. However, attempts to change the time step inside a simulation (for instance, switching to a smaller time step only during strong pulses) always resulted in spurious spikes in the output field at later points of the simulation. It may be, however, that adiabatic changes in time step could avoid these un-physical and undesired features.

## 4. Modeling

Early experimental observations of EID generally included a phenomenological model to attempt to quantify the loss of echo intensity. For instance, Huang et al. [7] introduced a Lorentzian distribution of random frequency shifts, $\rho(\varepsilon)$. Since these frequency shifts are introduced by the second pulse, after which the phase error simply accumulates until the photon echo occurs, the intensity of the photon echo should then decrease as (Eq. (3) of Ref. [7])

$$I_e \propto \left| \int_{-\infty}^{\infty} \rho(\varepsilon) \exp[-i\varepsilon t_{21}]\, d\varepsilon \right|^2. \tag{9}$$

This equation does well at predicting photon echoes of two brief pulses. Similar approaches were taken in other papers describing experimental observations of two-pulse photon echoes affected by EID [9,10,31,32]. However, since such treatments essentially quantify the simple graphical picture in Fig. 2, they are subject to the same limitations described there (no long pulses, no bandwidth effects, no propagation effects, and no chirps).

There have been previous attempts at modifying the Bloch equations to model effects similar to EID [33–35]. Shakhmuratov [34] and later, Asadullina [35], used modified values of $T_1$ and $T_2$ to reflect the additional dephasing contributions of random phase fluctuations that are either on the incident field, or which are induced in the sample by the presence of the incident field. Thus, this approach is suitable for experiments where the incident-field will remain constant, such as free-induction decay or hole burning. However, it is not clear how these approaches could be extended to photon echoes, unless it would be to simply switch between ordinary Bloch equations between pulses and the modified version during pulses.

Berman also modified the Bloch equations for relaxation in solids by adding a term in parallel to the $T_1$ and $T_2$ decay terms [33]. He was attempting to incorporate ordinary spectral diffusion (for

instance, due to random fluctuations in local magnetic-field) by modifying his version of Eq. (5) as

$$\frac{\partial r_1(z,t',\Delta)}{\partial t'} = \cdots - \frac{r_1(z,t',\Delta)}{T_2} + \int W(\Delta' \to \Delta)\, r_1(z,t',\Delta')\, \mathrm{d}\Delta', \text{etc.} \tag{10}$$

where $W(\Delta' \to \Delta)$ gives the "probability density per unit time that the local-field frequency shift undergoes a jump from" $\Delta'$ to $\Delta$ [33]. In the context of ordinary spectral diffusion, $W(\,)$ remains constant throughout the experiment and is only influenced by terms such as external magnetic field. What we show below is that this approach can be used for instantaneous spectral diffusion simply by allowing $W(\,)$ to vary continuously with the instantaneous change in local excitation. (In actuality, we developed our approach independently, and only later recognized the parallels with Ref. [33]).

To phenomenologically incorporate EID into the conventional Maxwell–Bloch equations, we stochastically impose random frequency jumps on each homogeneous ensemble of ions based on the overall excitation. After the usual evolution of the Bloch vector at each time step of the numerical simulation, all three components of the Bloch vector and the line shape $g(\Delta)$ for each detuning are scrambled with the Bloch vectors of neighboring detunings, by convolution with a Lorentzian kernel of narrow linewidth $\sigma_L$. Since these neighboring ions have randomized resonance frequencies, the width of this scrambler function is chosen at each time step as

$$\sigma_L = \sigma_{\mathrm{EID}} \int_{\forall \Delta} |r_3^t - r_3^{t-1}| g(\Delta)\, \mathrm{d}\Delta. \tag{11}$$

Because of the absolute value taken inside the integral, the scrambler width will always be greater than (or equal to) zero. Here, $\sigma_{\mathrm{EID}}$ represents a dimensionless scaling parameter that describes the strength of the EID. Thus, this one term incorporates the complex interplay between doping level, the distribution of ions due to doping, each ion's influence on the local field (change in permanent dipole moment between ground and excited states, etc.), and each ion's change in resonance frequency due to local field (Stark effect, etc.).

In essence, the instantaneous change in any ion's resonance frequency depends on the degree to which its local environment has changed, as quantified by the overall change in population. If not much excitation is occurring, then few ions are changing state and the narrow scrambler function has little impact. If some part of the simulated bandwidth is being strongly excited, then the resonance frequencies of all ions are more likely to undergo a significant random perturbation. These ions will then dephase from how they would have evolved at their original resonance frequency, leading to weaker photon echoes.

The advantage of our approach is that no assumptions are made as to how the EID will eventually influence the photon echo. The dephasing and rephasing of the various detunings occurs within the normal operation of the Maxwell–Bloch equations, so that any effects that emerge from long pulses, differences in pulse bandwidths, propagation effects or chirps will be included.

In the computer implementation, the convolution of Bloch vectors is implemented by using a fast Fourier transform (FFT) on the one-dimensional arrays of interest ($r_1$, $r_2$, $r_3$, and the line shape $g$—all functions of $\Delta$), followed by multiplication by the Fourier transform of a Lorentzian

$$\exp\left(-\left|\frac{2\pi\sigma_L u}{\Delta_{\min}}\right|\right), \tag{12}$$

where $u$ runs from $-0.5$ to 0.5 and $\Delta_{\min}$ is the sampling interval in the frequency domain (and thus the maximum extent in the transformed "time domain"). A second FFT returns the convolved copies of $r_1$, $r_2$, $r_3$, and $g$. For a rapid implementation, the complex-variable form of the "FFTW" algorithm is used twice [36,37], with two of the real-variable arrays carried each time (e.g., $r_1$ in the "real" part, $r_2$ in the "imaginary" part). To avoid unnecessary memory transfers, the $r_{1,2,3}$ variables remain within the custom FFTW memory structures throughout the simulation (e.g., during the implementation of the ordinary Bloch equations).

In all the simulations performed in this paper, such a small portion of the inhomogeneous line is

represented that the line shape parameter $g(\Delta) \sim 1$ for all $\Delta$. In this case, the weighting of the $r_{1,2,3}$ vectors by $g(\Delta)$ can effectively be ignored during the scrambling process. However, in other cases (e.g., for a relatively narrow inhomogeneous line width, or when a third state is trapping population out of the two-level system for persistent hole burning), it will be necessary to weight Eq. (11) with $g(\Delta)$ as shown, and in addition to consider the variation of $g(\Delta)$ when performing the convolution of the $r_{1,2,3}$ vectors. In such a situation, rather than multiplying $r_{1,2,3}$ by $g(\Delta)$ before each FFT operation (and then dividing it out afterwards), it may be more convenient to recast $r_{1,2,3}$ to include the $g(\Delta)$ term. This can be done by simply multiplying each side of Eq. (5) by $g(\Delta)$ and working with the terms $g(\Delta)r_{1,2,3}$. The variable $g(\Delta)$ still needs to be represented independently since it appears by itself (with $T_1$ in the third line of Eq. (5)).

Note that because the effects of EID are essentially incorporated within the underlying Bloch equations, the inclusion of EID into extensions of the Maxwell–Bloch model—for instance, to beams with Gaussian spatial profiles or to multiple beams of different angle of incidence [28,29]—should be relatively straightforward.

## 5. Simulations of photon-echo decays

Fig. 3 shows simulated photon echo decays without and with the EID feature enabled. A 1.0 μs pulse of area $\pi/2$ is followed at various delays by a 2 μs pulse of area $\pi$. For simplicity, results are shown for an optically thin media. To keep the simulated pulse bandwidths finite and thus avoid excessive ringing, all square pulses are given raised–cosine rising and falling edges (here spanning 25 ns) rather than instantaneous steps. $T_1$ and $T_2$ here are set to 2.0 ms and 400 μs, respectively. With a bandwidth of $\pm 15$ MHz and maximum time-span of 50 μs, 6000 frequency slots and 9500 time steps are used ($4\times$ and $2\times$ the minimum sampling discussed above) and the entire experiment represented in Fig. 3 (both with and without EID) took 7 min to run on a Pentium 1.1 GHz laptop. A simple trick, used here and throughout the rest of the paper, allowed us to greatly reduce the run-time for such photon echo decay curves. Note that the first 5 μs of all nine curves in a set is identical, and the next 5 μs are identical across eight of the nine sets, and so on. So these shared segments only need to be run once. After the simulator finishes the first photon echo from 0 to perhaps 20 μs, it restarts the simulation at that shared 5 μs branch-point to compute the second echo, and so on.

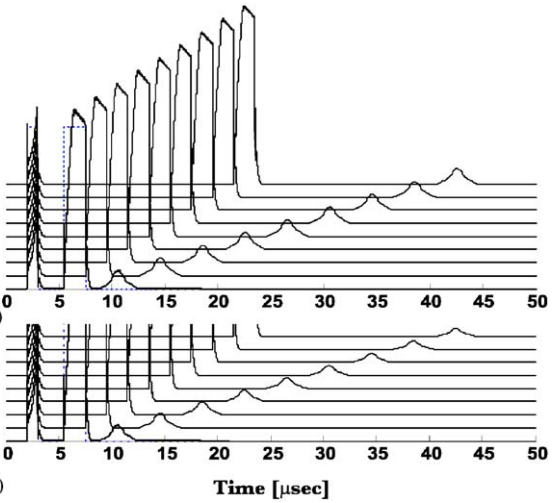


Fig. 3. Output intensity for simulated photon-echo decays are shown (a) without and (b) with the excitation-induced decay feature turned on ($\sigma_{EID} = 10^{-3}$). A 1.0 μs pulse of area $\pi/2$ is followed by a 2.0 μs pulse of area $\pi$, at increasing inter-pulse delays. These curves are run for an "optically thin" sample.

To calculate the effective photon echo decay curve, we can take either the peak value of the photon echo, or more typically, the energy density (the "area" under the photon echo intensity curve). The latter was computed by adding all the intensity—starting from, and on either side of, the peak of the photon echo—until the incremental energy added becomes smaller than 0.1% of the energy total. Fig. 4 shows such decay curves, each normalized to 1, for the two sets of simulated photon echo decays shown in Fig. 3. In the absence of EID, the photon echoes would be expected to decay with interpulse delay $t_{ab}$ as $\exp(-4t_{ab}/T_2)$, and the top curve does indeed follow this (for instance $\exp(-4 \times 20\ \mu s/400\ \mu s) \sim 0.8187$). However, in the presence

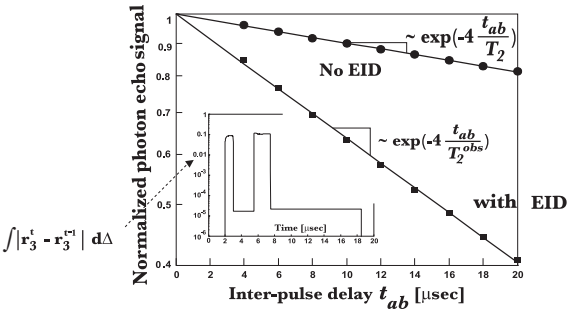


Fig. 4. Simulated photon-echo decay curves corresponding to the decays shown in Fig. 3, with and without the excitation-induced decay feature turned on. Here the normalized peak intensity values of the photon echoes are shown, although the area under the peak intensity (see text) produced quite similar decay curves. The observed value of $T_2$, termed here $T_2^{\text{obs}}$, is computed by fitting each decay to an exponential. In the "without EID" case, the exponential fit (solid line) does give the intrinsic value of $T_2$; with EID, a smaller value is observed (more rapid decay). The inset shows the time evolution of $\int |r_3^t - r_3^{t-1}| \, d\Delta$ as a function of time for the shortest decay, indicating the degree to which the Bloch vectors were scrambled during the simulation.

of EID the photon echo decay is much steeper, leading to an observed value of $T_2$—termed here $T_2^{\text{obs}}$—that is significantly smaller than the intrinsic value of $T_2$.

The inset of Fig. 4 describes how the modified Maxwell–Bloch simulator brings this about. The inset shows the value of $\int |r_3^t - r_3^{t-1}| \, d\Delta$ as a function of time for the shortest photon echo decay simulation. As expected, the largest changes in $r_3$ occur during the first and second pulse. Thus the most likely time for an ion to undergo a stochastic frequency hop is during these pulses, when neighboring ions absorb incident photons and move from the ground to the excited states, modifying their contribution to the local field. Since the two pulses are very similar in pulse area, on a log plot the change in $r_3$ is almost identical. However, as discussed above, the excitation during the second pulse has the dominant effect because that is when the phase excursions of the ions are largest (and thus a frequency hop can lead to the largest phase error at the photon echo). Note that once some excitation has occurred, there is always some low-level change in $r_3$, even between pulses and well after free-induction decay has died out. This is the $T_1$ decay of ions returning to their initial states, which in our model is simply additional change of excitation. Thus it would be straightforward to add the effects of "ordinary" spectral diffusion due to random magnetic spin-flips by simply increasing this time-independent background level. Such a continuous low level of scrambling leads to the non-exponential decays that are often seen in ordinary spectral diffusion [38,39].

## 6. Verification against experiment

While Fig. 4 shows that the modified Maxwell–Bloch simulator mimics the effects of EID, this verification is only in the qualitative sense. It would be much preferable to make *quantitative* comparisons between the new simulator and measured experimental data. For this, we turn to the literature.

In Refs. [7,8], Huang and co-workers in the Mossberg lab showed several experimental results (using the $^7F_0$–$^5D_0$ transition of 2 at% $Eu^{3+}$ in $Y_2O_3$) which convincingly demonstrated that photon-echo decays were subject to EID. For instance, in the experiment described in the inset of our Fig. 5(a), they performed four photon-echo decays between equal-area pulses (always $\pi/2$ followed by a $\pi$ pulse) at varying degrees of excitation, and observed more than a 5× change in observed time constant (from $T_2^{\text{obs}} \sim 228$ μs to 49 μs) [8]. Starting with a first (second) pulse of 1 μs (2 μs), they decreased the intensity of *both* pulses by factors of $F = 10$, 40, and 100 while simultaneously increasing the pulse durations by $\sqrt{F}$ (e.g., at constant pulse area). The experimental results, originally published as "Fig. 2" of Ref. [8], are shown as the dark lines in Fig. 5(a) and (b). The data was re-plotted here by extraction from a high-resolution scan of the original reference—even the scale on the vertical axis is retained. As would be expected, the large bandwidth addressed by the shortest pulses ($I_0$) causes significant EID, and thus leads to faster decays than the longer, low bandwidth pulses ($I_0/100$).

To match these curves, we repeatedly ran the Maxwell–Bloch–EID simulator with the

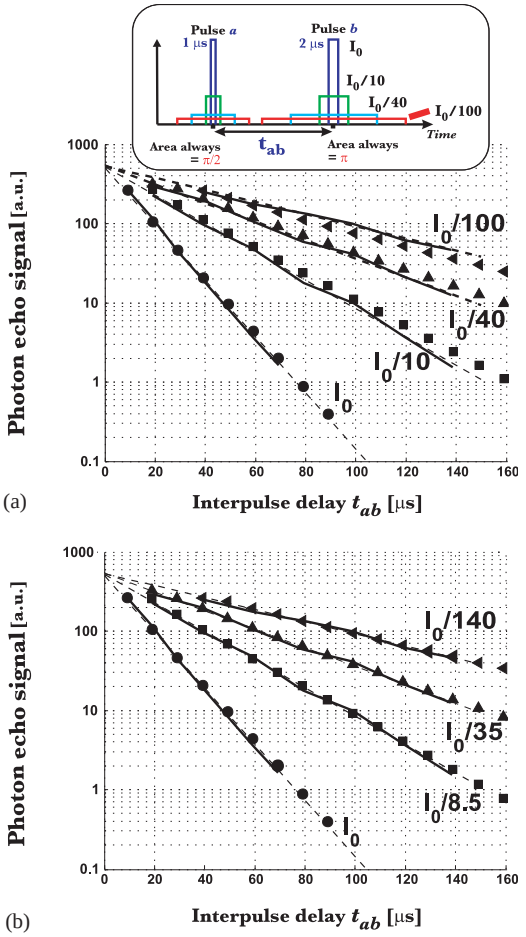


Fig. 5. (a) Comparison between published experimental photon-echo decays (black lines from Ref. [8], "Fig. 2") and numerical simulations using the EID-enabled Maxwell–Bloch algorithm introduced in this paper (filled symbols, $\sigma_{EID} \sim 4 \times 10^{-3}$, $T_1 = 860$ μs, $T_2 = 800$ μs). The inset describes the experiment, where two-pulse photon echo decays were measured for various reduced levels of excitation, implemented by increasing both pulse durations (from 1.0, 2.0 μs) by factors $F = 10, 40, 100$ while simultaneously decreasing the intensity by $\sqrt{F}$ (e.g., at constant pulse area). (b) Comparison between same experiment and simulation when a slightly different set of factors are used ($F = 8.5$, 35, 140), showing one plausible explanation for the slight discrepancies in part (a).

parameters of the "$I_0$" experiment, while varying our $\sigma_{EID}$ parameter. As one might expect, larger $\sigma_{EID}$ values lead to faster decays. Although the thickness of the crystal was given in Ref. [8], the absorption coefficient was not. Since we could not be sure of matching the effective optical thickness, we made the choice to run the simulator as if the sample was "optically thin" to keep the run-times tractable (even so, one decay curve from Fig. 5, with 16 000 steps along $\Delta$ and 25 000 time steps, takes nearly 4 h to run on a 2.4 GHz Pentium 4). Note that it was not necessary to know the precise intensities of the pulses used in the experiment: the simulator needs only the pulse area and duration. Once we found a value of $\sigma_{EID}$ that produced an excellent match with the lowest curve, we re-ran the simulator with the same value of $\sigma_{EID}$ but with the pulse durations and relative intensities corresponding to the three other curves ($I_0/10, I_0/40, I_0/100$). The results, shown by the filled symbols in Fig. 5(a), show strong agreement between the simulator and the experimental data. In fact, if slightly altered intensity values are used instead—reflecting perhaps values that might have actually been used in such a proof-of-principle experiment—then the match between simulation and experiment becomes nearly perfect (Fig. 5(b)).

A similar experiment, but with a much shorter second pulse, was performed in "Fig. 1(a)" of Ref. [7]. In a similar fashion, Figs. 6(a) and (b) show the match between simulated photon echo decay and the experiment, both with the intensity values listed in the paper (Fig. 6(a)) as well as with slightly altered intensity values (Fig. 6(b)). Note that the vertical and horizontal scales were chosen to match the published plot, although the simulated photon echo decays needed to be offset in time by 0.85 μs in order to correspond.

We should note that the match between simulation and experiment shown in Fig. 6 required a much lower value of $\sigma_{EID}$ than the later experiment (Ref. [8], our Fig. 5), despite the fact that the same crystal was likely used in both experiments. In addition, while we could obtain a fairly good match to the fastest non-exponential decay shown in "Fig. 1(b)" of Ref. [7] (same experiment, but brief pulse *first*, simulation not shown here), we were not able to then match the other two curves on that figure with the same $\sigma_{EID}$ conditions. At first, we attributed this to either the use of a different wavelength within the inhomogeneous line, or perhaps to inaccuracies in measuring the

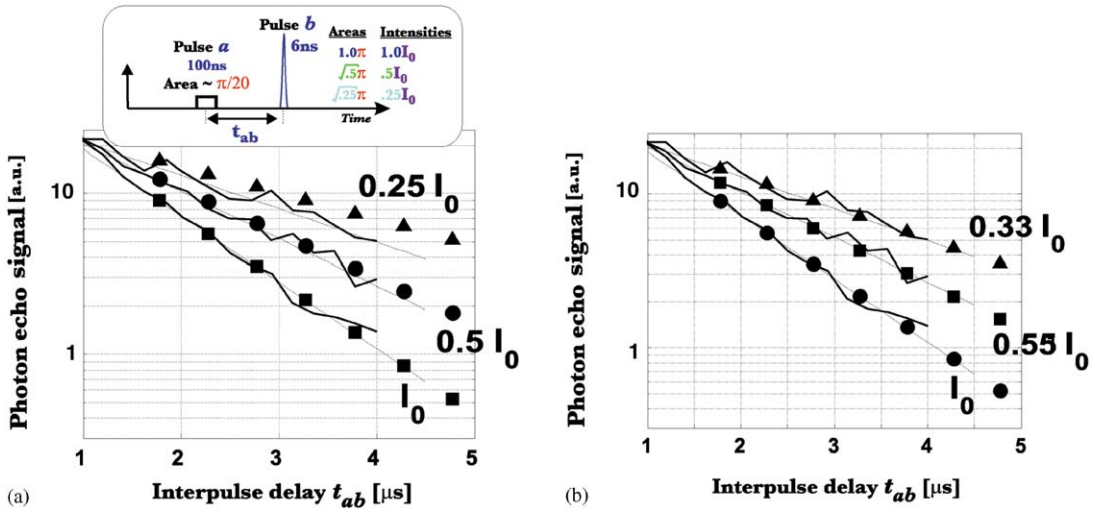


Fig. 6. (a) Comparison between published experimental photon-echo decays (black lines from Ref. [7], "Fig. 2(a)" and numerical simulations using the Maxwell–Bloch simulator with EID (filled symbols, $\sigma_{EID} \sim 4.4 \times 10^{-4}$, $T_1 = 860$ μs, $T_2 = 800$ μs). The inset describes the experiment—similar to Fig. 5 except that the second pulse is much shorter (6 ns). The discrepancy between the values of $\sigma_{EID}$ used here and in Fig. 5 is discussed in the text. (b) Improved comparison between experiment and simulation with slightly altered intensity-reduction factors.

6 ns pulse width of the brief amplified pulse. However, simulations run with different pulse width proved less accurate in matching the experimental data than the reported 6 ns value. And while changes in relative absorption coefficient would explain the change in $\sigma_{EID}$, it would not explain the failure to match "Fig. 1(b)" of Ref. [7]. Here, according to the simulator, the EID produced by the $T_1$ decay of the brief first pulse does produce non-exponential decays by itself, but this effect tended to get swamped by the normal EID-induced exponential decay caused by the longer second pulse. However, another potential explanation might be that in the experimental apparatus used in Ref. [7], the amplified 6 ns pulse was apparently not completely coherent with the longer gated pulses (e.g., this pulse was not bandwidth-limited) [40,41]. Thus, a significant part of the intensity of the brief pulse may not have been contributing to its effective area (as likely measured by its effectiveness in creating photon echoes with the second pulse). This could potentially explain both the lower $\sigma_{EID}$ value needed to produce Fig. 6 as well as the difficulty in matching "Fig. 1(b)" of Ref. [7].

Although the brief pulse used in the experiments of Ref. [7] may not have been completely coherent, this would not have been important when it was used as a scrambler pulse. Thus, we had no difficulty matching the experimental data from "Fig. 2" of Ref. [7], which is shown as the dark lines in Fig. 7. In this experiment, the two-pulse photon-echo intensity was measured as a function of the position of the intense brief pulse applied as a scrambler. As expected, when the scrambler coincides in time with the second pulse, then the photon-echo intensity is minimized. In Ref. [7], the detector was time-gated to keep the photon echoes produced by the amplified brief pulse away from the measured photon echo, and any lack of coherence would have helped minimize such crosstalk as well. In the simulation, we can easily add a scrambler by first running a simulation with just the brief pulse to capture the resulting evolution of $\int |r_3^t - r_3^{t-1}| \, d\Delta$. Then this additional dephasing contribution can be introduced (in addition to the usual population change generated internally) at any time-point within a second simulation, one which contains just the two pulses and the photon echo. Thus the scrambler pulse can

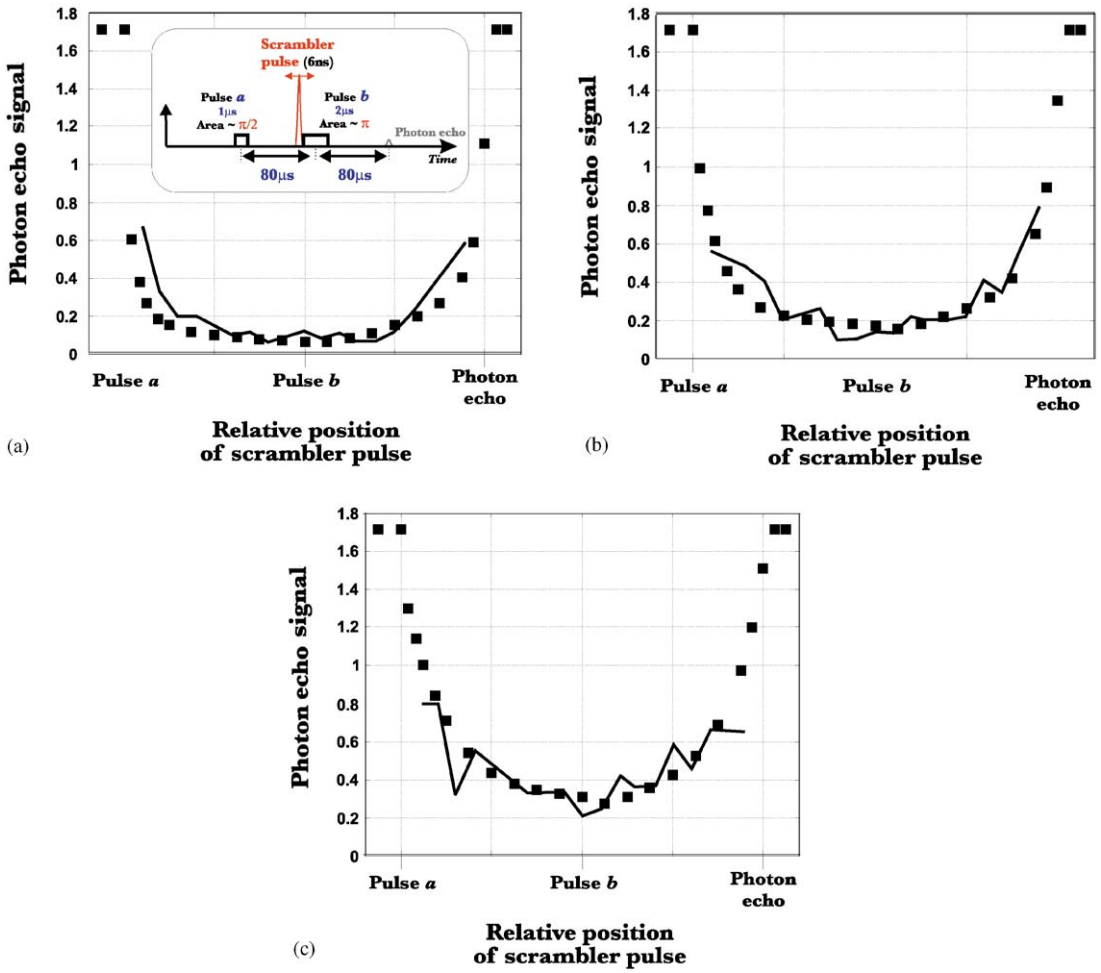


Fig. 7. (a) Comparison between published experimental photon-echo data [black lines from Ref. [7], "Fig. 1(a)" and numerical simulation (filled symbols, $\sigma_{EID} \sim 4.4 \times 10^{-4}$, $T_1 = 860$ μs, $T_2 = 800$ μs). Experiment corresponds to a two-pulse photon echo at fixed delay as a function of the position of a strong scrambler pulse. Plots (b) and (c) correspond to weaker ($I_0/2$, $I_0/4$) scrambler pulses.

be considered to be completely incoherent, or to be in a separate portion of the inhomogeneous line or even on a separate ion or site without needing to increase the time–bandwidth product of the photon-echo simulation. The filled symbols in Fig. 7 show the simulated photon-echo signal as a function of scrambler position, for three different scrambler intensities. The same vertical scaling parameter was used in all three curves.

Finally, the modified Maxwell–Bloch simulator can be used to match the experimental data shown at the beginning of the paper in Fig. 1(a). Here the ability of the Maxwell–Bloch simulator to handle chirps and optically thick media is used. Fig. 8 shows the simulation results (6600 steps in $\Delta$, 28 300 time-steps, 10 steps along $z$), showing reasonably good agreement between experiment and simulation. While the falloff of photon echo intensity with intensity for the two lower curves (higher bandwidth) is more gentle in the simulation than it is in the experimental data, all the right trends are present, and certainly the simulation results shown in Fig. 8 are far preferable to those in Fig. 1(b).

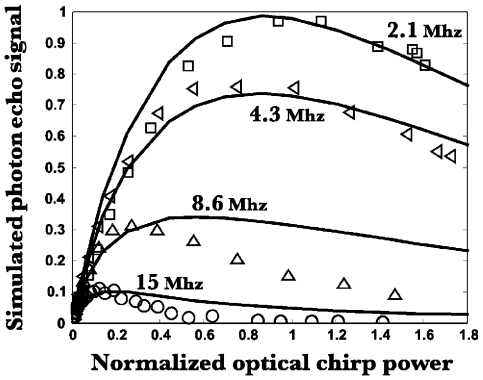


Fig. 8. Numerical simulation (solid lines) for the simple linear-chirp experiment (open symbols) described in Fig. 1. Simulation performed with $\sigma_{EID} = 2.5 \times 10^{-4}$, $T_1 = 2$ ms, $T_2 = 500$ μs, intensity $\alpha = 4.6$ cm$^{-1}$, and thickness = 0.26 cm.

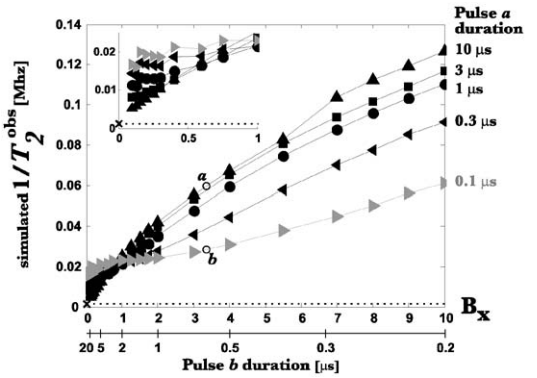


Fig. 9. Simulated photon echo decay constants, $1/T_2^{obs}$ versus "degree of excitation," for two-pulse photon echo decays where only the duration and intensity of the second pulse is varied at constant area (but otherwise identical to Fig. 5), for various first pulse durations (intensities). Pulse $a$ is always $\pi/2$ in area; pulse $b$ is always $\pi$. A similar experiment was performed in Ref. [8], "Fig. 3" in order to extrapolate to the intrinsic value of $T_2$—parameters here are chosen to correspond to this experiment. The $\times$-mark and dotted line at $1/T_2^{obs} = 0.00125$ MHz represents the "correct" value of $T_2 \sim 800$ μs. Points $a$ and $b$ are identified for use in comparing to Fig. 10. Lines are present only to guide the eye.

## 7. Extrapolating to the intrinsic value of $T_2$

One of the problems with EID is that it can mask the intrinsic value of $T_2$, the portion of the dephasing time that is independent of excitation intensity. Measuring this parameter is important when studying spectrally sensitive materials, as it reveals information about the homogeneous line width and the nature of the homogeneous broadening. Thus, the presence of EID complicates experiments where one would like to measure the underlying dephasing time, or to study the dephasing mechanisms through the variation in $T_2$ with various parameters (such as external electric or magnetic field).

In order to obtain the intrinsic value of $T_2$, "Fig. 3" of Ref. [8] performed a linear fit to the inverse of the measured decay rates ($1/T_2^{obs}$) as a function of the degree of excitation ($B_x \sim 1/\sqrt{F}$). (This experiment was identical to the one described in Fig. 5, except that only the second pulse was varied). The intuition is that as the excitation approaches zero, so will the effects of EID, revealing the intrinsic value of $T_2$. The question we address here with our Maxwell–Bloch EID simulator is not the basic intuition (which our results do not dispute), but whether such a linear fit can produce an accurate estimate of $T_2$. In so doing, we discovered some unexpected effects that seem to depend on the relative bandwidths of the first and second pulse.

In Fig. 9, we show the inverse of the observed dephasing time taken from simulated photon-echo decays, $1/T_2^{obs}$, as a function of the duration of the second pulse, for various different values of the first pulse. All simulations were run "optically thin". For each data point, the exponential time constants shown were fitted to photon-echo decays containing 3–4 points, using the same time range for all decays. In this region, the decays do appear to be exponential; however, similar simulations hint that some of these decays should become somewhat non-exponential at longer delay times. We do not consider this added complication here. At the extremes of the simulated range of pulse durations, the numerical experiments become difficult for much the same reasons that would occur in actual experiments: photon echoes that are weak (from either low excitation or very rapid decay) are difficult to measure accurately; conversely, when the two pulses are long yet closely spaced, the photon echoes are

hard to distinguish from the free-induction decay of the second pulse.

According to Fig. 9, only the longest first pulses seem to give data that could be linearly extrapolated to the intrinsic value of $T_2$ (set for simulations to 800 μs, or $1/T_2 = 1.25$ kHz (0.00125 MHz)). Certainly, this method (varying the second pulse at constant area) may not be the best way to estimate $T_2$. To try to understand this, we reversed the experiment: varying the duration of the first pulse for various different values of the second pulse. The results, shown in Fig. 10, may provide yet another explanation why some experiments find that the first pulse has no impact on EID (the center curve in Fig. 10, for instance), while others show it does have an impact (other two curves in Fig. 10).

We have labelled the same two operating points in both Figs. 9 and 10 to attempt to help explain these strange effects. At point *a* in Fig. 10, the photon-echo decays much faster than at point *b* even though the second pulse is exactly the same. However, the narrow bandwidth of the first pulse at *a* means that when the short (0.6 μs) second pulse arrives, it finds many of the ions that it is addressing to be still in the ground state, leading to large changes in $r_3$ as the $\pi$ pulse excites these ions straight to the excited state. In contrast, at point *b*, these same ions addressed by the short second pulse—having already been affected by the short first pulse—are at or near $r_3 = 0$. Here, the second pulse writes a frequency grating to encode the time delay, but the overall change in $r_3$ is much smaller, neighboring ions do not change as much and thus there is less EID (slower decays). We did not find such a straightforward explanation for the opposite trend on the bottom curve, but we expect that it is also related to the relative bandwidths addressed by the two pulses. Note that the point at which the first pulse has little impact on the photon echo decay rate is when the first and second pulses are nearly equal in duration (bandwidth). It would be interesting to see if these relative-bandwidth-dependent effects could be observed experimentally.

In terms of obtaining the intrinsic value of $T_2$, perhaps a more accurate experiment to determine the intrinsic (e.g. non-EID) value of $T_2$ might be to keep the pulse durations constant rather than area. This avoids changing any bandwidths during the experiment, and is also how more recent measurements than Ref. [8] have been done Ref. [42,43]. Fig. 11 shows the simulated photon echo decay

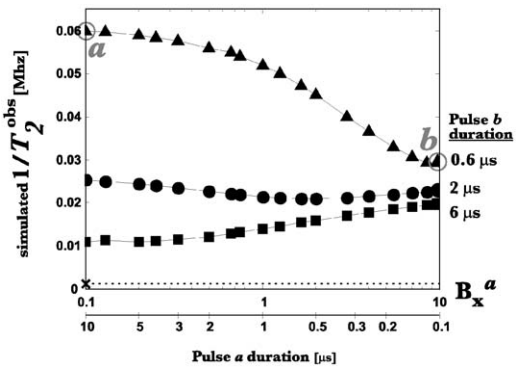


Fig. 10. Simulated photon echo decay constants, $1/T_2^{obs}$ versus "degree of excitation," for two-pulse photon echo decays where only the duration and intensity of the *first* pulse is varied at constant area (the complement to Fig. 9), for various second pulse durations (intensities). Points *a* and *b* here correspond to points *a* and *b* in Fig. 9. Lines are present only to guide the eye.

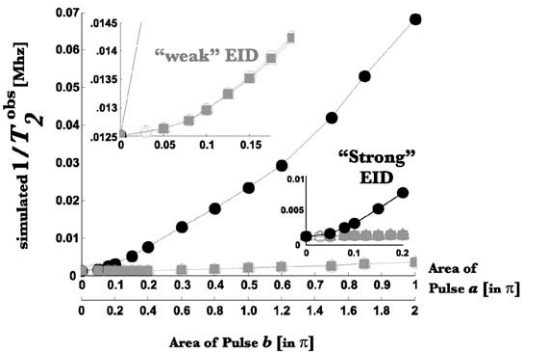


Fig. 11. Simulated photon echo decay constants, $1/T_2^{obs}$ versus pulse area, for two-pulse photon echo decays where the intensity of both pulses is varied at constant duration, for both weak ($\sigma_{EID} \sim 10^{-4}$, gray symbols) and strong ($\sigma_{EID} \sim 4 \times 10^{-3}$, black symbols) levels of EID. Insets magnify the intersection with the vertical axis to illustrate the difficulty of extrapolating to the "correct" $1/T_2$ in the presence of any amount of EID, unless only the weakest photon echo measurements are used. Open symbols show that varying $T_1$ from its original value of 860 μs either down to 400 μs or up to 8 ms has little effect on the simulated photon echo decays. Lines are present only to guide the eye.

constants for such an experiment. Here the duration of the first (second) pulse is always 1 μs (2 μs) and the intensities are equal (e.g., area of second pulse is always twice that of the first pulse). Clearly, even close to the origin, a linear fit does not extrapolate to the correct intrinsic value of $T_2$, nor is the evolution even smoothly quadratic. In the case of a small amount of EID (upper inset of Fig. 11), then only when sufficient data are available for pulse areas below $\pi/20$ will a linear fit give the correct answer. However, even including data up to $\pi/10$ will lead to an error in estimating $T_2$. And since $T_1$ has little impact (open symbols), this is not purely the aftereffects of the earlier excitation.

There appear to be two ways around this. The first, already known to researchers in the field [40], is to convert the horizontal axis from pulse area to "excitation density." In this way, the extrapolation is then linear in the number of ions excited. However, while this makes qualitative sense, it is not clear how one should actually calculate this "excitation density." For instance, as we saw above, the excitation caused by the second pulse (which is assumably responsible for most of the EID effects) is not necessarily the same when following a first pulse of significant area as it would be in isolation. However, to keep things simple, we chose to simply convert from pulse area to "excitation density" by integrating under the $r_3$ versus $\Delta$ curve after an isolated pulse. But we are trying to compare to what an experimentalist would do with their data. So rather than use the full Maxwell–Bloch simulation, we simply took the area under the Fourier transform of the pulse as seen through the expected cosine nonlinearity. This approach is really only valid near zero excitation, but fortunately this is exactly the region of interest here. Therefore, excitation density is simply

$$\mathscr{E}_{\mathscr{D}} = \int 1 - \cos\left(A\pi \frac{\sin(\pi\Delta)}{\pi\Delta}\right) \mathrm{d}\Delta, \qquad (13)$$

where $\Delta$ is the frequency relative to the center of the pulse and $A$ is the area of the pulse in units of $\pi$. The resulting curve is shown in Fig. 12. Note that by normalizing the vertical axis, we remove any dependence on the absolute pulse bandwidth.

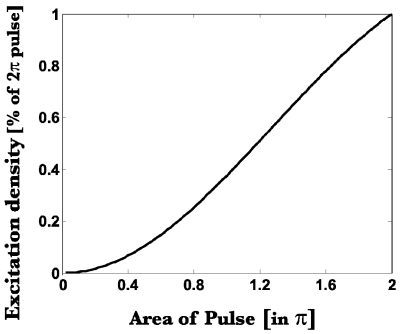


Fig. 12. Plot of "excitation density," or the total change in $r_3$ due to a single pulse, as a function of the pulse area in units of $\pi$. Plot is normalized to the total excitation created by a $2\pi$ pulse in order to make it independent of bandwidth.

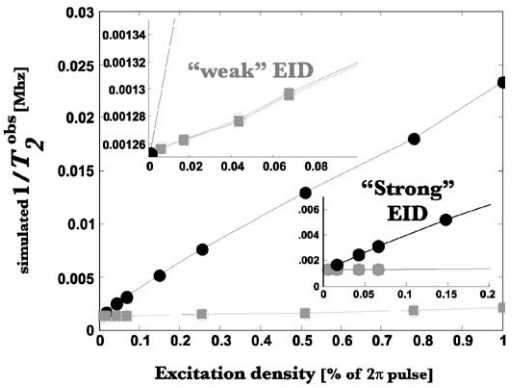


Fig. 13. Data from Fig. 11, with horizontal axis rescaled by Fig. 12, e.g., simulated photon echo decay constants, $1/T_2^{\mathrm{obs}}$ versus "excitation density." By converting from pulse area to "excitation density," it becomes possible to extrapolate to the "correct" $1/T_2$ in the presence of varying amounts of EID. Lines are present only to guide the eye.

Using this definition of "excitation density," we scaled the horizontal axes from Fig. 11 and replot the same data in Fig. 13. Here it is clear that the correct intrinsic value of $T_2$ can be obtained for either "weak" or "strong" EID.

The second method we found to avoid the incorrect extrapolation of Fig. 11 was to change the experiment so that only the area of the *second* pulse varied. The first pulse remained fixed in both area and duration, and as above, the second changes only in intensity at constant duration. As

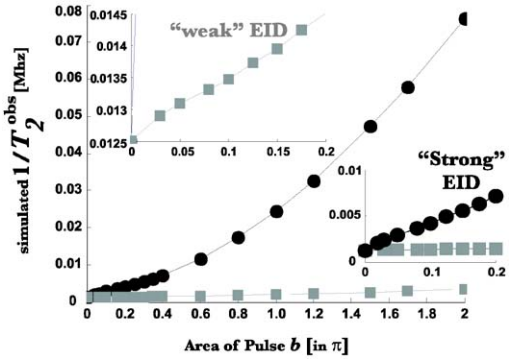


Fig. 14. Simulated photon echo decay constants, $1/T_2^{obs}$ versus area of the second pulse, for two-pulse photon echo decays where the intensity of only the second pulse is varied at constant duration, for both weak ($\sigma_{EID} \sim 10^{-4}$, gray symbols) and strong ($\sigma_{EID} \sim 4 \times 10^{-3}$, black symbols) levels of EID. The first pulse is kept at an area of $\pi/4$. Insets magnify the intersection with the vertical axis to illustrate that it is possible to accurately extrapolate to the "correct" $1/T_2$ in the presence of either level of EID. Lines are present only to guide the eye.

shown in Fig. 14, this also produces an experiment that gives the "correct" value of the intrinsic value of $T_2$, but *only* when the horizontal axis is given in pulse area. Scaling to "excitation density" as shown in Fig. 12 is the wrong thing to do here, since the incremental change in excitation from a low-area second pulse after a significantly large first pulse is not the same as if the low-area pulse had been applied in isolation. Thus, this second method bypasses the ambiguity about how "excitation density" gets quantified, at the cost of a more complicated experiment (two closely spaced pulses set to arbitrary intensities rather than simply time-gating a beam of constant intensity).

The extrapolation to "zero" excitation in order to obtain an accurate estimate of $T_2$ thus would seem to call for constant duration experiments (no variations in bandwidth), and either careful attention to how the degree of excitation actually applied is quantified, or the use of only a single varying parameter (for instance, just the area of the second pulse). In both cases, however, the EID-enabled Maxwell–Bloch simulator proves useful in quantifying intuition and by revealing subtle emergent effects.

## 8. Discussion

There is (at least) one discrepancy between our approach and the underlying physics: the convolution described above is a memory-less random walk, whereas the modification of the local neighborhoods by excitation is eventually reversed slowly by $T_1$ decay. Fortunately, since signal strengths also die rapidly with $T_1$ and times of interest are usually $\ll T_1$, this is often not an issue. However, some two-species experiments have been performed with photon echoes generated on a long $T_1$ ion species or site, and scrambler pulses on a second (but spatially co-located) species of much shorter $T_1$ [19,44]. In such a situation, our model would not predict the results accurately. However, the much more common scenario of EID due to the lingering (but slow) $T_1$ decay from an earlier strong scrambler pulse will be modeled correctly.

In order to correctly simulate the random walk with memory, it would be necessary to be able to return each portion of Bloch vector that had been scrambled to a nearby detuning to its original detuning, but *with* its "share" of all the changes that had occurred to the neighbor detuning. While this would be intractable to do directly, it is possible that one could track the collective average of the "lent-out" portion of each Bloch vector. In addition, the integral $\int |r_3^t - r_3^{t-1}| \, d\Delta$ would need to be treated in two parts: the portion where $r_3^t - r_3^{t-1} > 0$ so that excitation is proceeding from ground to excited (leading to pure scrambling, as in this paper), and the transition from excited back to ground ($r_3^t - r_3^{t-1} < 0$, leading to "unscrambling" or the re-coalescing of Bloch vectors back to their "home" resonance frequencies).

In addition, this work was motivated by and checked against experimental results for photon echoes in media doped with rare-earth ions (specifically, Eu). Phenomena present in other types of spectrally sensitive material may require adaptations to this approach.

Possible avenues for future work that have been opened up by this work might include:

(1) experimental investigation of the pulse bandwidth effects described in Section 7,

(2) simulation of free-induction decay in the presence of EID, perhaps validated by matching to either optical or spin experiments [18,45],
(3) connection with underlying physical models of ion–ion coupling, where $\sigma_{EID}$ is derived from basic parameters such as doping level and distribution, the position within the absorption line, permanent dipole moments, and Stark coefficient (or other similar effects known to lead to frequency-shifts with changes in local field),
(4) the tie-in described above with intrinsic but time-evolving dephasing effects such as ordinary spectral diffusion, the "frozen core" [46–48], etc.,
(5) connection with quantum-computing schemes [20,21], where the stochastic scrambler is replaced with specific frequency jumps due to a countable number of relevant neighbors, and
(6) engineering optimization of bandwidth and degree of excitation to maximize data storage/processing performance in the presence of EID.

## 9. Conclusions

We have described the incorporation of EID into the numerical simulation of photon echoes. At each time step of the numerical integration of the Bloch equations, we model the stochastic frequency jumps of ions caused by excitation of neighboring ions by convolving the Bloch vectors with a narrow scrambling kernel. The width of this convolution kernel follows the instantaneous change in overall population, integrated over the simulated bandwidth. The advantage of our approach is that by introducing EID at a very basic level, we avoid any *a priori* assumptions about its impact. This has allowed us to find emergent effects that have not been described elsewhere (or admittedly, observed experimentally yet). In addition, we can model complex scenarios of practical import including data-bearing pulses, chirped pulses, and optically thick materials.

We validated our modifications of the Maxwell–Bloch model by extensive comparison against published and original experimental results, including two-pulse photon echo decay curves, photon echoes perturbed by short scrambling pulses, and chirped excitation pulses. An analysis of the accuracy of various experimental methods for extrapolating to the intrinsic $T_2$ in the presence of EID, and new emergent behavior related to the relative bandwidths of the first and second incident pulse, were also described.

The incorporation of EID into Maxwell–Bloch modeling should offer both improved understanding of experimental results, as well as more substantive analysis of engineering tradeoffs allowing more aggressive design-points in realistic optical coherent transient applications.

## Acknowledgements

The authors would like to acknowledge many helpful discussions with Roger Macfarlane, Bob Shelby, and John Hoffnagle of the IBM Almaden Research Center, and with Tiejun Chang, Mingzhen Tian, and Professor Rufus Cone of Montana State University.

## References

[1] M.D. Levenson, IBM Techn. Disclosure Bull. 7 (6) (1981) 2797.
[2] T.W. Mossberg, Opt. Lett. 7 (2) (1982) 77.
[3] Y.S. Bai, W.R. Babbitt, N.W. Carlson, T.W. Mossberg, Appl. Phys. Lett. 45 (7) (1984) 714.
[4] W.R. Babbitt, T.W. Mossberg, Opt. Commun. 65 (3) (1988) 185.
[5] D.R. Taylor, J.P. Hessler, Phys. Lett. A 50 (3) (1974) 205.
[6] G.K. Liu, M.F. Joubert, R.L. Cone, B. Jacquier, J. Lumin. 38 (1–6) (1987) 34.
[7] J. Huang, J.M. Zhang, A. Lezama, T.W. Mossberg, Phys. Rev. Lett. 63 (1) (1989) 78.
[8] J. Huang, J.M. Zhang, T.W. Mossberg, Opt. Commun. 75 (1) (1990) 29.
[9] G.K. Liu, R.L. Cone, Phys. Rev. B 41 (10) (1990) 6193.
[10] M. Mitsunaga, T. Takagahara, R. Yano, N. Uesugi, Phys. Rev. Lett. 68 (21) (1992) 3216.
[11] R.M. Macfarlane, R.S. Meltzer, J. Phys. 46 (C-7) (1985) 253.
[12] Y.S. Bai, R. Kachru, Phys. Rev. B 46 (21) (1992) 13735.

[13] J.R. Klauder, P.W. Anderson, Phys. Rev. 125 (3) (1962) 912.
[14] D.R. Taylor, J.R. Marko, I.G. Bartlet, Solid State Commun. 14 (3) (1974) 295.
[15] F. Bloch, Phys. Rev. 70 (7–8) (1946) 460.
[16] R.L. Shoemaker, Coherent transient infrared spectroscopy, in: J.I. Steinfeld (Ed.), Laser and Coherence Spectroscopy, Plenum Press, New York, 1978, pp. 197–371.
[17] A.G. Redfield, Phys. Rev. 98 (6) (1955) 1787.
[18] R.G. Devoe, R.G. Brewer, Phys. Rev. Lett. 50 (17) (1983) 1269.
[19] S.B. Altner, G. Zumofen, U.P. Wild, M. Mitsunaga, Phys. Rev. B 54 (24) (1996) 17493.
[20] M. Nilsson, L. Levin, N. Ohlsson, T. Christiansson, S. Kroll, Phys. Scripta T102 (2002) 178.
[21] N. Ohlsson, R.K. Mohan, S. Kroll, Opt. Commun. 201 (1–3) (2002) 71.
[22] M.A. Nielsen, I.L. Chuang, Quantum Computation and Quantum Information, Cambridge University Press, Cambridge, UK, 2000.
[23] T.L. Harris, C.M. Jefferson, G.W. Burr, J.A. Hoffnagle, M. Tian, W.R. Babbitt, J. Opt. Soc. Am. B, to appear.
[24] R.W. Olson, H.W.H. Lee, F.G. Patterson, M.D. Fayer, J. Chem. Phys. 76 (1) (1982) 31.
[25] M. Azadeh, C.S. Cornish, W.R. Babbitt, L. Tsang, Phys. Rev. A 57 (6) (1998) 4662.
[26] C.S. Cornish, Highly efficient photon echo generation and a study of the energy source of photon echoes, Ph.D. Thesis, University of Washington, 2000.
[27] R.R. Reibel, High bandwidth optical coherent transient true-time delay, Ph.D. Thesis, Montana State University, 2002.
[28] T. Chang, M. Tian, W. R. Babbitt, in these Proceedings (HBSM 2003), J. Lumin. 107 (2004).
[29] T. Chang, M. Tian, Z.W. Barber, W.R. Babbitt, in these Proceedings (HBSM 2003), J. Lumin. 107 (2004).
[30] Tiejun Chang, Montana State University, personal communication.
[31] J. Huang, J.M. Zhang, A. Lezama, T.W. Mossberg, J. Lumin. 45 (1–6) (1990) 392.
[32] G.K. Liu, R.L. Cone, M.F. Joubert, B. Jacquier, J.L. Skinner, J. Lumin. 45 (1–6) (1990) 387.
[33] P.R. Berman, J. Opt. Soc. Am. B 3 (4) (1986) 564.
[34] R.N. Shakhmuratov, F.M. Gelardi, M. Cannas, Phys. Rev. Lett. 79 (16) (1997) 2963.
[35] N.Y. Asadullina, T.Y. Asadullin, Y.Y. Asadullin, J. Phys.: Condens. Matter 13 (22) (2001) 5231.
[36] M. Frigo, S.G. Johnson, The fastest fourier transform in the west, Technical Report MIT-LCS-TR-728, September 1997.
[37] FFTW-the Fastest Fourier Transform in the West, www.fftw.org (2000).
[38] W.B. Mims, Phys. Rev. 168 (2) (1968) 370.
[39] R.M. Macfarlane, T.L. Harris, Y. Sun, R.L. Cone, R.W. Equall, Opt. Lett. 22 (12) (1997) 871.
[40] Rufus Cone, Montana State University, personal communication.
[41] Thomas Mossberg, LightSmyth Technology, personal communication.
[42] R.W. Equall, Y. Sun, R.L. Cone, R.M. Macfarlane, Phys. Rev. Lett. 72 (14) (1994) 2179.
[43] G.M. Wang, R.W. Equall, R.L. Cone, M.J.M. Leask, K.W. Godfrey, F.R. Wondre, Opt. Lett. 21 (11) (1996) 818.
[44] F.R. Graf, B.H. Plagemann, A. Renn, U.P. Wild, M. Mitsunaga, Opt. Lett. 22 (3) (1997) 181.
[45] R. Boscaino, F.M. Gelardi, J.P. Korb, Phys. Rev. B 48 (10) (1993) 7077.
[46] R.M. Shelby, C.S. Yannoni, R.M. Macfarlane, Phys. Rev. Lett. 41 (25) (1978) 1739.
[47] R.M. Macfarlane, R. Wannemacher, D. Boye, Y.P. Wang, R.S. Meltzer, J. Lumin. 48–49 (1991) 313.
[48] A. Szabo, J. Lumin. 58 (1–6) (1994) 403.